GOES 8 retrieval of dust aerosol optical thickness over the Atlantic Ocean during PRIDE

Jun Wang,[1] Sundar A. Christopher,[1] Jeffrey S. Reid,[2,3] Hal Maring,[4] Dennis Savoie,[4] Brent N. Holben,[5] John M. Livingston,[6] Philip B. Russell,[7] and Shi-Keng Yang[8]

Received 29 April 2002; revised 2 August 2002; accepted 17 December 2002; published 31 July 2003.

[1] Using 30 days of half-hourly, high temporal resolution GOES 8 imager data and radiative transfer calculations, dust aerosol optical thickness (AOT) was retrieved over the Atlantic Ocean (14°N ~ 26°N, 73°W–63°W) during the Puerto Rico Dust Experiment (PRIDE). Dust aerosol size distributions and complex index of refraction inferred from ground-based measurements (1.53–0.0015i at 0.55 μm), which were used in Mie calculations and a plane-parallel discrete ordinate radiative transfer model (DISORT) to compute look up tables for AOT retrievals. Using a combination of spectral, spatial, and temporal tests, a dust detection algorithm was developed from the GOES 8 imager data. The degradation of the signal response relative to the prelaunched calibration of the GOES 8 visible channel was 39% in July 2000 and the GOES 8 AOT detection limit was estimated to be 0.04 in AOT (0.67 μm). The satellite-retrieved AOT were then compared with AOT values derived from ground-based Sun photometer (SP) sites. The comparison showed that GOES 8 retrieved AOT are in good agreement with the SP derived values, with linear correlation coefficient of 0.91 and 0.80 for the two sites. The GOES 8 monthly mean 0.67 μm AOT (0.19 ± 0.13, 0.22 ± 0.12) over the two SP sites matched the monthly mean SP AOT values (0.23 ± 0.13, 0.22 ± 0.10). The linear correlation between the GOES 8 retrieved AOT and the aircraft derived values from particle probe data and airborne Sun photometer AATS-6 measurements were 0.88 and 0.83, respectively. Besides the uncertainties from the nonspherical effect of dust aerosols, sensitivity studies showed that the uncertainties ($\Delta\tau$) of the GOES 8 retrieved AOT values were mainly from the uncertainties due to the imaginary part of refractive index ($\Delta\tau = \pm 0.05$) and surface reflectance [$\Delta\tau = \pm(0.02 \sim 0.04)$]. This paper demonstrates the application of geostationary satellites to detect and retrieve dust AOT even at low to moderate AOTs. The GOES 8 imager with high temporal resolutions also captures aerosol diurnal variation in this study that can further reduce the uncertainties in the current aerosol forcing estimations caused by the high temporal variations of AOT, thereby playing a complementary role with global AOT retrievals from polar orbiting satellites. *INDEX TERMS:* 0305 Atmospheric Composition and Structure: Aerosols and particles (0345, 4801); 3359 Meteorology and Atmospheric Dynamics: Radiative processes; 3360 Meteorology and Atmospheric Dynamics: Remote sensing; *KEYWORDS:* dust aerosol, diurnal optical depth, GOES 8, radiative forcing

Citation: Wang, J., S. A. Christopher, J. S. Reid, H. Maring, D. Savoie, B. N. Holben, J. M. Livingston, P. B. Russell, and S.-K. Yang, GOES 8 retrieval of dust aerosol optical thickness over the Atlantic Ocean during PRIDE, *J. Geophys. Res.*, *108*(D19), 8595, doi:10.1029/2002JD002494, 2003.

[1]Department of Atmospheric Sciences, University of Alabama in Huntsville, Huntsville, Alabama, USA.
[2]Atmospheric Propagation Branch, SPAWAR System Center, San Diego, California, USA.
[3]Now at Naval Research Laboratory, Monterey, California, USA.
[4]Rosenstiel School of Marine and Atmospheric Science, University of Miami, Miami, Florida, USA.
[5]Biospheric Sciences Branch, NASA Goddard Space Flight Center, Greenbelt, Maryland, USA.
[6]SRI International, Menlo Park, California, USA.
[7]NASA Ames Research Center, Moffett Field, California, USA.
[8]Climate Prediction Center, National Centers for Environmental Prediction, Washington, D. C., USA.

0148-0227/03/2002JD002494$09.00

1. Introduction

[2] Dust aerosols are major contributors to aerosol loading in the atmosphere [*D'Almeida*, 1987]. The global source strength of dust aerosols is estimated to be 1000–5000 million tons per year [*Duce*, 1995]. Aerosol particles perturb the Earth radiation budget and hence climate through two different mechanisms. Aerosols directly affect the extinction of solar and infrared radiation by the scattering and absorption processes in the atmosphere. Aerosols also affect the formation and microphysics of clouds by serving as cloud condensation nuclei (CCN) [*Twomey*, 1977; *Kaufman and Nakajima*, 1993], thus producing an

indirect effect on the Earth's energy budget. Because of the high spatial and temporal variations of dust aerosols and their properties, it is difficult to quantify the direct radiative effect [*Fouquart et al.*, 1987; *Claquin et al.*, 1998; *Liao and Seinfeld*, 1998]. Therefore large uncertainties still exist in the assessment of dust radiative effects on climate [*Sokolik and Toon*, 1996; *Intergovernmental Panel on Climate Change* (*IPCC*), 2001]. Estimation of global radiative forcing by mineral dust ranges from -0.6 to $+0.4$ W m^{-2} [*IPCC*, 2001]. The magnitude and sign of the direct radiative effect of dust aerosols on climate, is still uncertain [*Fouquart et al.*, 1987; *IPCC*, 2001, *Hasen and Lacis*, 1990].

[3] Satellite measurements, because of their large spatial coverage and continuous observations, are a useful tool for detecting aerosols and retrieving aerosol properties [e.g., *Stowe et al.*, 1997]. The global aerosol optical thickness (AOT) over the ocean has been retrieved from one visible channel (ch1) of the advanced very high resolution radiometer (AVHRR) [*Rao et al.*, 1989; *Ignatov et al.*, 1995], two channels of AVHRR [*Wagener et al.*, 1997; *Mishchenko et al.*, 1999; *Higurashi and Nakajima*, 1999], two channels of the visible and infrared scanner (VIRS) [*Ignatov and Stowe*, 2000] and two UV channels of the Total Ozone Mapping Spectrometer (TOMS) [*Torres et al.*, 2002]. Recently, both multispectral data from the Moderate Resolution Imaging Spectrometer (MODIS) and four-wavelength multiangle data from Multiangle Imaging Spectroradiometer (MISR) have been used to retrieve the global AOT over ocean and land [*Tanré et al.*, 1997; *Kaufman et al.*, 1997; *Chu et al.*, 2002; *Diner et al.*, 2001]. Current AOT retrievals from polar orbiting satellites are able to capture aerosol outbreaks from various regional sources such as dust aerosols from the Sahara desert and smoke aerosols from South America and South Africa [*Jankowiak and Tanré*, 1992; *Higurashi and Nakajima*, 1999; *Christopher et al.*, 2000]. Although polar orbiting platforms are useful for retrieving aerosol properties, their low temporal resolution ($\sim$1 or 2 views per day of a given site) makes it difficult to capture the diurnal aerosol variations. *Levin et al.* [1980] reported that the dust AOT (at wavelength 0.65 μm) could change by a factor of two in less than two hours during the passage of a dust front. Further uncertainties in the current retrievals also result from the assumed aerosol refractive index [*Claquin et al.*, 1998], size distributions [*Tegen and Lacis*, 1996], shape [*Mishchenko et al.*, 1997], measurement calibrations, and surface reflectance [see *King et al.*, 1999, and references therein].

[4] The new generation of GOES imagers [*Menzel and Purdom*, 1994] have improved spatial and spectral capabilities that can be used for cloud property retrievals [e.g., *Greenwald and Christopher*, 2000], biomass burning fire detection [e.g., *Prins et al.*, 1998] and smoke AOT retrieval [e.g., *Zhang et al.*, 2001; *Christopher and Zhang*, 2002; *Christopher et al.*, 2002; *Knapp et al.*, 2002]. One distinct advantage of geostationary satellites is the high temporal resolution when compared to polar orbiting satellites. The major goal of this paper is to demonstrate the ability of geostationary satellite measurements from the GOES 8 imager for detecting dust aerosols and retrieving their AOT. Specifically, aerosol refractive index of dust aerosols that was used in our radiative transfer calculations is derived through Mie calculations by using size distributions measured from the ground and the light scattering measurements made during PRIDE. Dust AOT values are retrieved from GOES 8 imager data by using a look-up table (LUT) approach [*Zhang et al.*, 2001; *Christopher and Zhang*, 2002]. The GOES 8 retrieved AOT are then compared with the Sun Photometer (SP) AOT values from the Aerosol Robotic Network (AERONET) [*Holben et al.*, 1998] and the 6-channel Ames Airborne Tracking Sunphotometer (AATS) AOT values from aircraft [*Livingston et al.*, 2003]. Finally, sensitivity studies are used to estimate the uncertainties in the GOES 8 retrieved AOT due to assumptions in refractive index, size distribution, and surface reflectance.

2. Data and the Area of Study

[5] In July 2000, the Puerto Rico Dust Experiment (PRIDE) was conducted in Puerto Rico and its vicinity [*Reid et al.*, 2003a]. One of the major goals of this field experiment was to study the radiative properties of dust aerosols that were transported from the Saharan desert to the Puerto Rico region. The measurements are described in *Reid et al.* [2003a].

[6] The ground-measured aerosol size distributions and their optical properties, such as scattering and absorption coefficients, were obtained from two particle sizers and aerosol light scattering and absorption measurements, respectively. The two particle sizers cover a range from 0.003 to 15 μm with 152 spectrum intervals, and measure the aerosol size distributions every 20 min. Aerosol light scattering was measured using TSI© Integrating Nephelometer Model 3563 [*Anderson et al.*, 1996]. The instrument performs a geometrical integration of the angular distribution of scattered intensity, such that scattering coefficient of the air (molecular plus aerosols) can be measured with the combination of a Lambertian light source and an orthogonal light detector [*Anderson et al.*, 1996]. This instrument was calibrated weekly using carbon dioxide [*Maring et al.*, 2000]. Light scattering data was corrected for instrument nonidealities using the method outlined by *Anderson and Ogren* [1998]. Aerosol light absorption was measured by making measurements of diffuse reflectance off high volume bulk aerosol filters.

[7] During the PRIDE field campaign, dust particle vertical distributions were regularly measured in the vicinity of Puerto Rico by the SSC-SD Navajo on twenty-one flights during the 28 June through 24 July study period [*Reid et al.*, 2003a]. The Navajo carried navigational, pressure, temperature, and dew point instrumentation and also used wing mounted Particle Measuring Systems (PMS) Forward Scattering Spectrometer Probe (FSSP-100), and a Passive Cavity Aerosol Spectrometer Probe (PCASP-100X). Nominally, the PCASP and FSSP measure particle sizes between 0.1–3.0 μm and 0.75–18 μm, respectively. However, as discussed by *Reid et al.* [2003b], optical particle counters suffer from severe sizing errors when measuring coarse mode dust (diameters > 2 μm), and here the FSSP is used as a coarse mode particle counter only to give the relative vertical distribution of the dust. The SSC-SD Navajo was also equipped with the six-channel NASA Ames Airborne Tracking Sunphotometer (AATS-6) to measure aerosol optical thickness at 380, 451, 526, 864, and 1021 nm plus water vapor (940 nm band) [*Matsumoto et al.*, 1987;

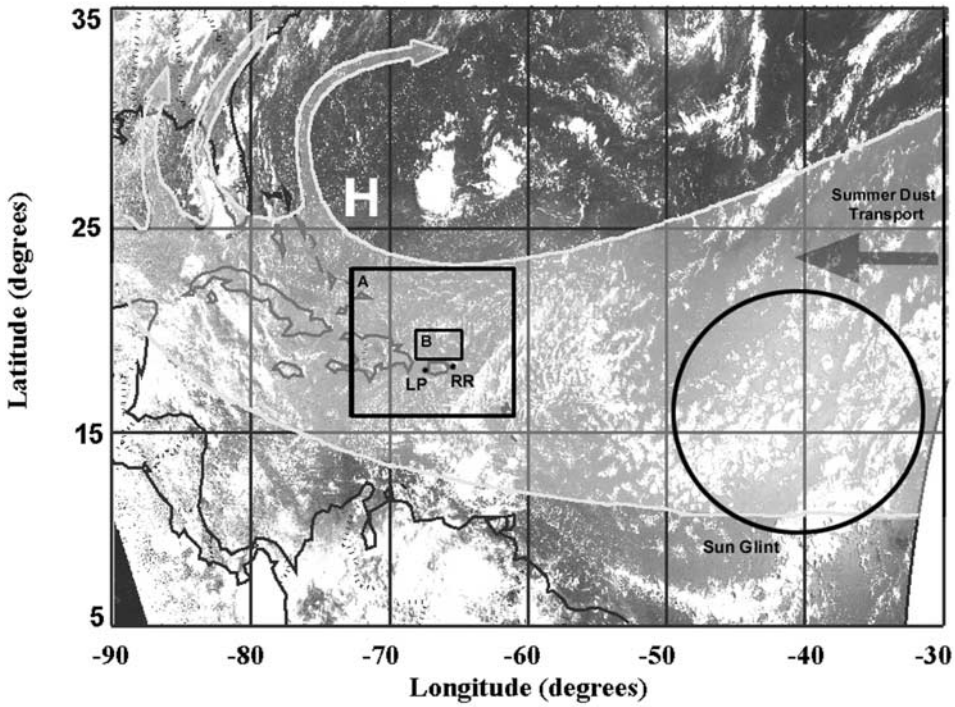

Figure 1. Enhanced GOES 8 ch1 image on 28 June 2000 at 1145 UTC. The conceptual model [*Rapp*, 1976] shows how dust from Africa can be transported into the continental United States as it circulates clockwise around the semipermanent "Bermuda" high-pressure zone (H) [*Perry et al.*, 1997]. Also shown are the Sun glint area (circle) and two study areas (box A and B, see text). The two SP measurements at La Paguera (marked as point LP) and Roosevelt Road (marked as RR) reported an AOT of 0.5 on this day.

Livingston et al., 2003]. Vertical profiles of AOT can yield bulk light extinction coefficients during cloud free conditions. To account for contamination by cirrus and some cumulus clouds, and to improve vertical resolution, PMS probe data was used with airborne AOT data as a constraint to derive aerosol extinction coefficients.

[8] Half-hourly GOES 8 data at 13 time periods (1301, 1331, 1401, 1431, 1531, 1601, 1631, 1701, 1731, 1901, 1931, 2001 and 2031 UTC) from 28 June to 26 July 2000 were used (data at 1501, 1801, and 1831 UTC were not available). The GOES 8 imager has channels with half-power response bandwidths of 0.52–0.72 μm (channel 1), 3.79–4.04 μm (channel 2), 6.47–7.06 μm (channel 3), 10.2–11.2 μm (channel 4) and 11.6–12.5 μm (channel 5). The instantaneous geometric field of view (IGFOV) is 1.0 × 1.0 km in channel 1 and 4.0 × 4.0 km in channel 4 and channel 5. The derived sampled subpoint spatial resolution (SSR) of channel 1 is 0.57 × 1 km and for channel 4 and channel 5 is 2.3 × 4 km [*Menzel and Purdom*, 1994].

[9] The visible band of GOES 8 has no on board calibration, and has undergone signal degradation due to the accumulation of material on the scanning mirror [*Ellrod et al.*, 1998]. The calibration uncertainty in the visible band is found to be one of the largest sources of error in aerosol optical thickness retrievals [e.g., *Geogdzhayev et al.*, 2002]. However, previous studies have successfully retrieved cloud and aerosol properties from the GOES imager by using proper vicarious methods for estimating the effect of degradation [*Greenwald and Christopher*, 2000; *Zhang et al.*, 2001; *Christopher and Zhang*, 2002]. In this study, we account for the GOES 8 visible channel signal degradation using the calibration formula recommended by *Rao et al.* [1999]. The degradation ratio (i.e., one minus the ratio of reflectance using the prelaunch coefficient to that using the postlaunch coefficient) of 39% was used.

[10] The total column AOT (quality assured, version 2.0) derived from two AERONET sites, Roosevelt Road (RR, 18.20°N, 65.60°W) and La Paguera (LP, 17.97°N, 67.05°W), are used to compare against the GOES 8 retrieved AOT values. The AERONET SPs measure direct solar radiation at 340 nm, 380 nm, 440 nm, 500 nm, 670 nm, 870 nm, and 1020 nm [*Holben et al.*, 1998]. The measured solar radiance is then used to infer the column AOT by using a cloud screening process and an inversion algorithm based on Beer-Lambert-Bouguer Law [*Smirnov et al.*, 2000; *Holben et al.*, 1998]. The attenuation due to Rayleigh scattering and the absorption of ozone are estimated and removed. The uncertainty in the retrieved AOT is on the order of 0.01 [*Holben et al.*, 1998; *Smirnov et al.*, 2000].

[11] Figure 1 shows a GOES 8 ch1 image from 28 June 2000 at 1145 UTC. Also, superimposed on this image is the conceptual model of the summer dust transport [*Rapp*, 1976; *Karyampudi et al.*, 1999]. The area of study is shown in the rectangle marked as A. During the summer months, dust from Africa is transported into the continental United States as it circulates clockwise around the semipermanent "Bermuda" high-pressure zone (denoted by H in Figure 1) [*Rapp*, 1976; *Westphal et al.*, 1987; *Perry et al.*, 1997; *Karyampudi et al.*, 1999]. The two SP sites at LP and RR both reported AOT values of 0.5 at 0.67 μm on this day.

Figure 1 also shows the Sun glint area and another study area marked as B that was used to study the GOES 8 dust detection limit (see section 4).

3. Methodology

[12] Our retrieval method is based on a look-up table (LUT) approach [*Zhang et al.*, 2001; *Christopher and Zhang*, 2002; *Christopher et al.*, 2002]. Radiative transfer calculations are used to precompute the radiance as a function of AOT for a range of Sun-satellite viewing geometry and surface reflectance values. The dust AOTs are retrieved when the best fit is obtained between the GOES 8 reflectance of dust pixels and the LUT reflectance.

[13] The sea surface reflectance is inferred from the clear sky reflectance at the top of atmosphere (TOA) by using a minimum composite method [*Moulin et al.*, 1997; *Zhang et al.*, 2001]. The glint geometry is filtered out based on the *Cox and Munk* [1954] model calculations, in which a typical sea surface wind of 7 m s^{-1} was assumed that is also a good approximation for PRIDE [*Reid et al.*, 2003a]. The uncertainties in obtaining sea surface reflectance and its effect on the GOES 8 AOT retrievals are discussed in section 6.

[14] Dust optical properties are determined by dust complex refractive index, size distribution, and the shape of particles. Because of the large temporal and spatial variability of aerosol properties [*Levin et al.*, 1980; *Schütz and Jaenicke*, 1974], there are uncertainties in the current aerosol optical depth retrieval methods [*King et al.*, 1999]. Both the size distribution and refractive index of dust aerosols can change during the transport of dust from Africa due to preferential loss of larger particles, sea salt mixing [*Patterson et al.*, 1977] or NSS (non-sea-salt) sulfate mixing [*Savoie et al.*, 1989]. The inferred imaginary part of the refractive index (N_i) of pure Saharan dust decreased from 0.009 to 0.002 (at 0.5 μm) due to mixing with sea salt aerosols during the transport process from Africa to Barbados (13.13°N, 59.41°W) near the surface in the marine boundary layer (MBL) [see *Patterson et al.*, 1977, Figure 4]. The dust particle size depends on the prevailing meteorological conditions such as wind speed and humidity [*Schütz and Jaenicke*, 1974] and the distance from its source because of deposition or the gravity effect [*Patterson*, 1981]. For instance, 75% of the large particles (>10 μm) of dust aerosols from the Sahara desert can be redeposited in the source area, leaving 25% to reach the ocean 1500 km away. [*Schütz and Jaenicke*, 1974].

[15] Previous studies have shown that dust aerosols over Puerto Rico are neither typically marine nor continental in nature [*Volz*, 1970]. The dust aerosols are usually mixed with marine aerosols [*Savoie et al.*, 1989]. The ground-based size distribution measurements during PRIDE show that the dust aerosols over Puerto Rico have a larger fraction of small particles (less than 1 μm) and a smaller fraction of large particles (larger than 1 μm) compared to the dust aerosols in the Saharan source regions in different meteorological conditions (e.g., sand storm, wind carried, and background, Figure 2). The observed size distributions are shown in the inset of Figure 2, where the solid lines represent days when the SP retrieved AOT were larger than 0.4 and shaded lines represent days when the SP measured AOT were smaller than 0.2. Figure 2 shows that when AOT

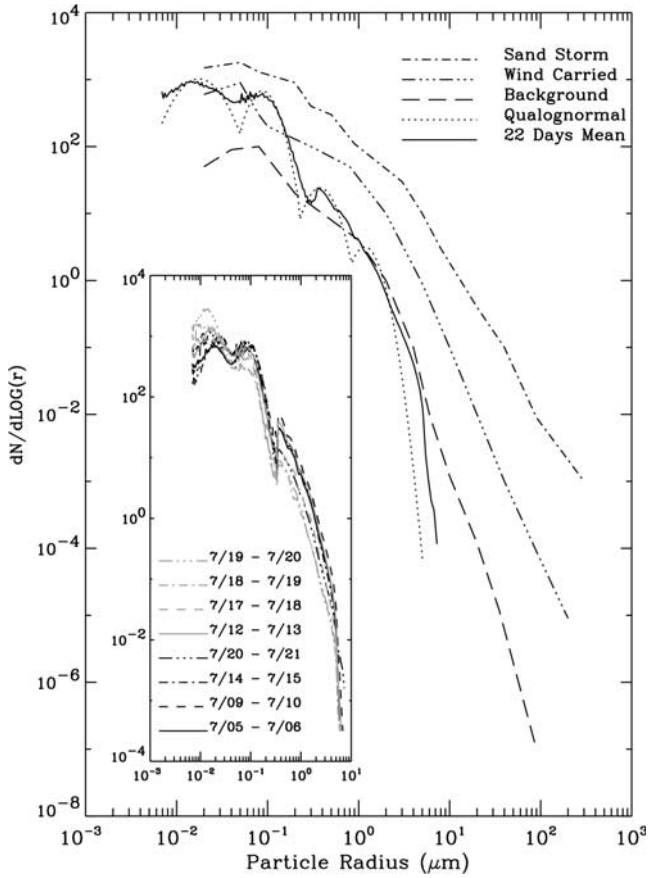

Figure 2. Averaged dust aerosol size distribution observed over 22 days during PRIDE. A qualognormal size distribution is derived from these observations (as shown by the dotted line). Also shown are three other Sahara dust aerosol distributions [*D'Almeida*, 1987].

becomes larger, the number of particles with radius larger than 1μm are also larger, implying that dust is a major component of the increased AOT. The averaged size distribution from 22 days and three trilognormal size distributions for dust aerosols in Sahara desert in different meteorological conditions [*D'Almeida*, 1987] are also shown in Figure 2. In this study, the measured mean size distribution from 22 days is converted to a qualognormal distribution (dotted line in Figure 2) using the formula suggested by *Davies* [1974]:

$$\frac{dNC_i(r)}{d\log r} = \frac{NC_i}{\sqrt{2\pi}\log\sigma_i}\exp\left(-\frac{(\log r - \log r_g)^2}{2(\log\sigma_i)^2}\right), \qquad \frac{dNC(r)}{d(\log r)} = \sum_{i=1,4}\frac{dNC_i(r)}{d(\log r)} \tag{1}$$

where r_g is geometric mean radius, σ is the standard deviation, $NC_i(r)$ is the number concentration corresponding to *i*th mode. The four geometric radii (r_g) are 0.02 μm, 0.09 μm, 0.38 μm, and 1.2 μm respectively with corresponding σ values of 1.71, 1.40, 1.42, and 1.37, and corresponding percentage of each mode (NC_i/NC) is 69.972%, 28.829%, 1.072%, and 0.127%. The derived qualognormal (qualognormal indicates that there are four single lognormal modes

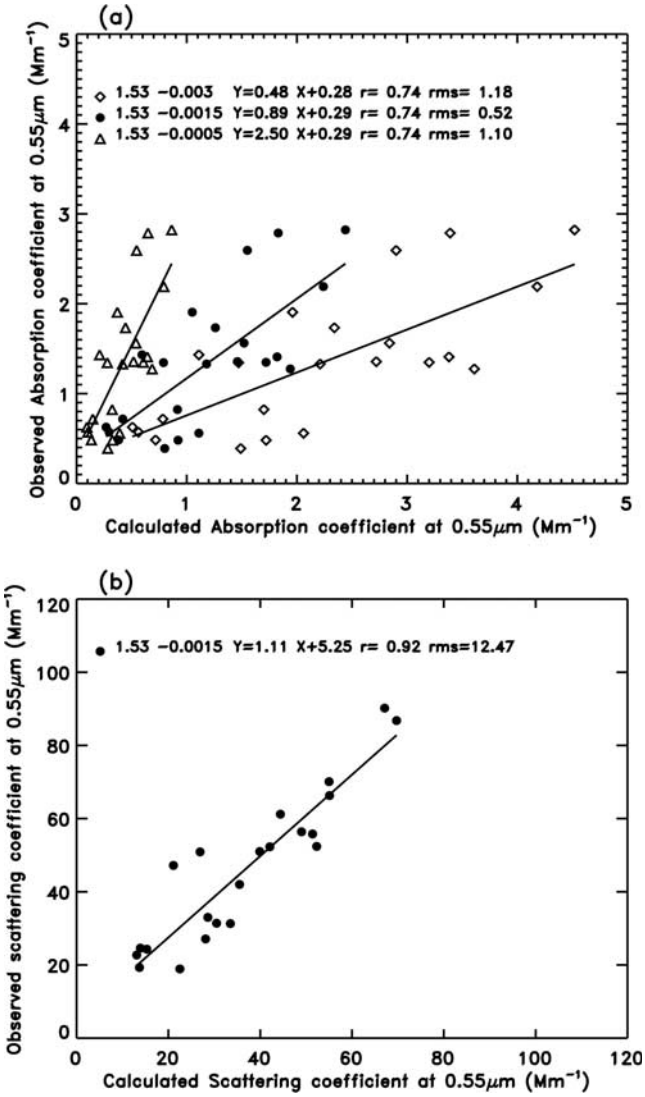

Figure 3. (a) Scatterplot of observed dust absorption coefficient with calculated absorption coefficient for different refractive index. (b) Scatterplot of observed dust scatter coefficient with calculated scatter coefficient for refractive index of 1.53−0.0015i. (Mm = 10^6 m).

as defined in equation (1) to compose the whole size distribution) size distribution produces an effective radius (r_{eff}) value of 0.72 μm. The value of r_{eff} is smaller than that of continental dust (e.g., from 1.5 μm to 2.5 μm [*Kaufman et al.*, 2001]) but is similar to results (0.6 μm) from a previous study over Puerto Rico [*Volz*, 1970].

[16] The refractive index of dust aerosols is not well known, and several discrepancies in the current literature have been reported [e.g., *Sokolik et al.*, 1993; *Kaufman et al.*, 2001]. Previous studies used the dust aerosol refractive index suggested by *Patterson et al.* [1977] that yielded a single scattering albedo (ω_0) value of 0.80 at 0.6 μm [*D'Almeida*, 1987]. The mean N_i of Patterson's refractive index between 0.3 μm and 0.70 μm is 0.008, in which there is a strong dependence on the wavelength (e.g., N_i is 0.025 at 0.3 μm and 0.0038 at 0.7 μm) [*Patterson et al.*, 1977]. The World Climate Program (WCP) value of the dust refractive index is 1.53−0.008i [*WCP*, 1983], that is similar to the Patterson refractive index. *Moulin et al.* [1997] found the best agreement between Meteosat- and Sun photometer-derived dust optical thickness when the refractive index is 1.5−0.01i. Recently, using the Sea-viewing Wide Field-of-view Sensor (SeaWiFS) satellite data and the Simulation of the Satellite Signal in the Solar Spectrum (5S) radiative transfer model [*Moulin et al.*, 2001], a value of 1.53−0.001i for the Saharan dust over the Atlantic Ocean has been used. A refractive index value of 1.53−0.001i at 0.67 μm in the visible band is also used by *Kaufman et al.* [2000] to retrieve the AOT for Saharan dust over land. With such small values of N_i, the ω_0 calculated from Mie theory is larger than 0.95 when using several typical size distributions summarized by *Moulin et al.* [1997]. High values of ω_0 (0.97 at 0.64 μm) were also inferred from both ground measurements and satellite measurements [*Kaufman et al.*, 2001].

[17] In this paper, we derive the refractive index of dust mixed aerosols by fitting calculated radiative properties to ground measurements. Since the daily dust size distribution was available during PRIDE, we calculated the dust absorption coefficient from Mie theory using a range of different values of the imaginary part of the dust refractive index (Figure 3a). We then compared the calculated results with the observed absorption coefficients from ground-based measurements. Figure 3a shows that the refractive index value of 1.53−0.0015i at 0.55 μm provides the best agreement with the observed values. The comparison between the observed scattering coefficient (σ_{obs}) and the calculated scattering coefficient (σ_{cal}) using a refractive index value of 1.53−0.0015i has a linear correlation coefficient of 0.92 with the equation:

$$\sigma_{cal} = 1.11 \times \sigma_{obs} + 5.25 \quad (2)$$

[18] Although the calculated scattering coefficient values are highly correlated with the measured scattering coefficient values, Mie calculations underestimate the total measured scattering coefficient about 20%. Our calculations also show that a change of ±0.03 in real part of refractive index (N_r) from a nominal value of 1.53 will lead to a change in calculated scattering coefficient within 2%, which still underestimate the measured scattering coefficient even after considering the maximum measurement uncertainties (10% [*Anderson et al.*, 1996]). *Maring et al.* [2000] also reached similar conclusions for the dust aerosols over Canary Island, and ascribed this underestimation to the nonspherical shape of dust particles. Observation has shown that dust aerosols are not entirely spherical [*Kalashnikova and Sokolik*, 2002; *Mishchenko et al.*, 1995]. Such nonspherical effect can result in large errors in the satellite AOT retrievals, especially at certain scattering angles [*Mishchenko et al.*, 1997]. However, since current parameters for aspect ratio and particle shape of nonspherical particles are very limited, we assumed that the dust particles were spherical, and used a refractive index value 1.53−0.0015i at 0.55 μm in our aerosol model. The uncertainty in our retrievals due to the nonspherical effect and the refractive index is discussed in section 6.

[19] For the GOES 8 visible channel, under cloud free conditions, the radiative processes contributing to the measured radiance are gas absorption, the scattering process in the atmosphere (Rayleigh scattering and Mie scattering), and

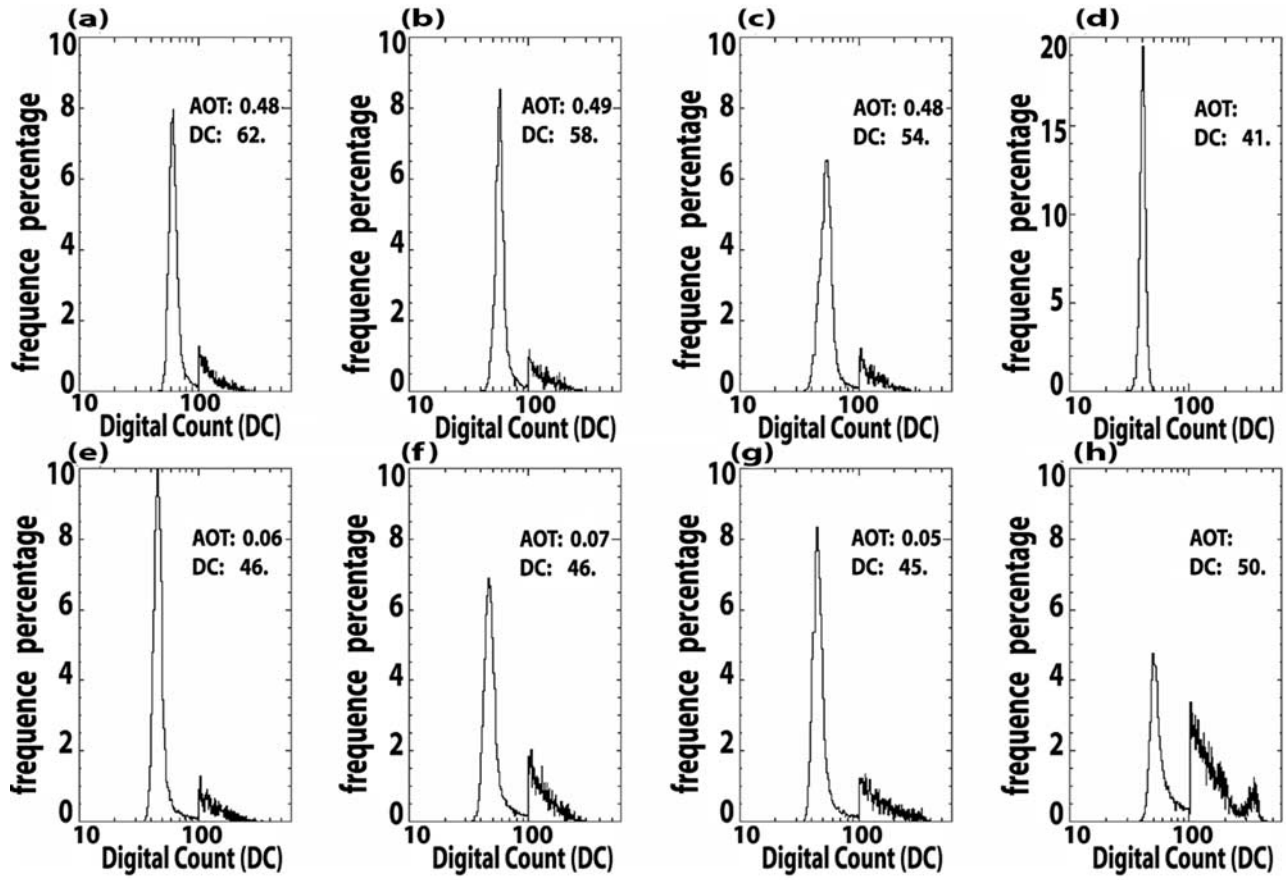

Figure 4. Histogram of ch1 raw digital count value at 1301 UTC on heavy dust loading (AOT > 0.48) and light dust loading (AOT < 0.1) events at 1301 UTC on (a) 28 June 2000, (b) 29 June 2000, (c) 21 July 2000, (d) clear sky from the monthly mean composite, (e) 11 July 2000, (f) 19 July 2000, (g) 24 July 2000, and (h) 3 July 2000. The AOT values are from the SP measurements. The frequency for DG larger than 100 has been amplified 100 times for display purposes.

the scattering processes at the surface. In this study, a discrete ordinate radiative transfer (DISORT) model [*Ricchiazzi et al.*, 1998] was used to consider the multiple scattering processes. A typical tropical profile [*McClatchey et al.*, 1971] with total water vapor of 4.117 gcm^{-2} and total ozone of 0.253 atm-cm were used. Since GOES 8 ch1 covers a spectral range of 0.22 μm, the spectral response function of the GOES 8 imager was used in the radiative transfer calculations. The refractive index at 0.67 μm is 1.53 – 0.001i and the effective ω_0 is 0.98 in GOES ch1 wavelength spectrum. Those results are similar to those used in previous studies (e.g., 1.58 – 0.002i at 0.69 μm [*Carlson and Benjamin*, 1980]; ω_0 of 0.95 [*Fouquart et al.*, 1987]). The aerosol radiative parameters (ω_0, extinction coefficient and the Legendre coefficient of the aerosol phase function) from Mie calculations are then input to the DISORT model. Several values ranging from a pure molecular atmosphere (AOT = 0) to a very turbid atmosphere (AOT = 2) [*Tanré et al.*, 1988] were considered in the construction of the LUT.

4. Dust Detection Using the GOES 8 Imager

[20] To retrieve dust AOT, we must first remove clouds from the GOES 8 imager data. We then define the dust detection limit as the minimal AOT (τ) required to produce an increment of one digital count (DC) for clear sky over seawater (i.e., $d\tau/dDC$) [*Moulin et al.*, 1997]. Figure 4 shows the histogram of the GOES 8 DC values at 1315 UTC for different days with different dust loading conditions (i.e., for SP measured AOT > 0.48 and AOT < 0.1) in the box marked as B in Figure 1. For comparison purposes, the histogram of DC in cloud-free and cloudy conditions are also shown in Figures 4d and 4h, respectively. The AOT value from SP measurements and the peak DC values are also shown in each figure. The peak DC value increases when AOT increases. The peak DC and AOT (τ) have a linear correlation coefficient of 0.79 with the equation:

$$\tau = 0.043DC - 1.885 \quad (3)$$

[21] We therefore estimated that the dust detection limit for GOES 8 during PRIDE is 0.04. When compared to the Meteosat 4 detection limit of 0.06 [*Moulin et al.*, 1997], the GOES 8 detection limit is better due to the higher radiometric resolution (10 bits) of the GOES 8 visible imager compared to Meteosat (6 bits).

[22] If the increased DC is converted to reflectance, the ch1 reflectance increases by about 2.5% ~ 3.5% due to dust

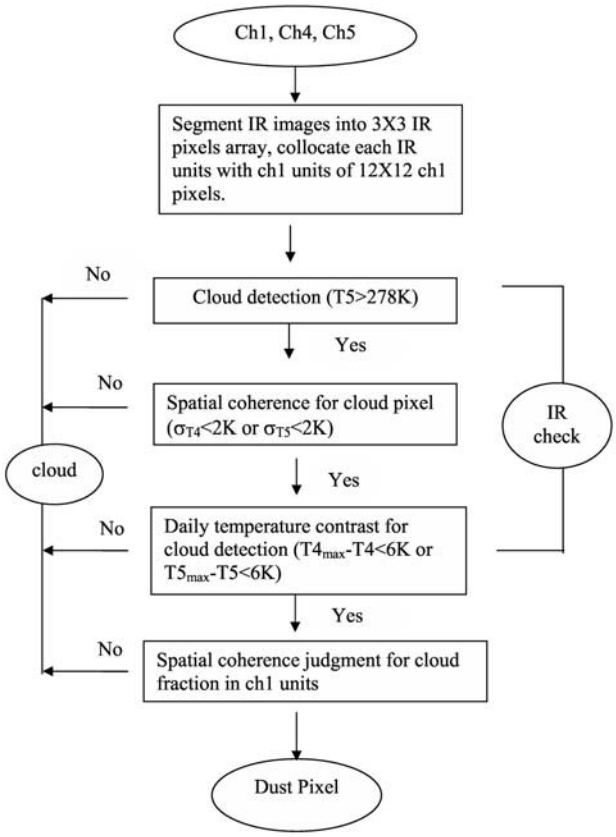

Figure 5. Flowchart showing the cloud clearing procedure for GOES 8.

aerosol loading. This enhanced effect is small when compared to the effect of dust near the coast of Africa [*Liu et al.*, 2003]. The histogram of the GOES 8 ch1 reflectance in Figure 4 shows that the reflectance of dust pixels is about 7% but always less than 15%. As an example, the reflectance of cloudy pixels on 3 July 2000 was around 30%. The clear sky TOA ocean reflectance estimated from the minimum composite method ranges from 1% to 5% with most values centered around 3.3%. The above analysis shows that the signature of dust aerosols from GOES 8 imagery over the Puerto Rico region is small, making satellite detection of dust aerosols a challenging task even over a dark ocean background.

[23] Since the dust AOT over Puerto Rico was less than 0.5 during the study period (based on SP measurements), the dust signature was not very pronounced in infrared or visible imagery. Therefore it is necessary to develop a reliable technique to identify dust aerosols from the GOES 8 imager. We used a combination of ch1, ch4 and ch5 along with spatial and temporal tests. Figure 5 shows the steps used in identifying dust aerosols. First, the GOES 8 channel 4 and channel 5 images are segmented into 3×3 arrays. A ch5 brightness temperature (T5) threshold test is first used. A pixel is labeled as cloudy if $T5 < 278$ K in the 3×3 array. The second test checks for the standard deviation of ch4 (σ_{T4}) and ch5 (σ_{T5}) brightness temperature values. If σ_{T4} or σ_{T5} is larger than 2K, this 3×3 array is classified as cloudy. The third test uses a daily temperature contrast. First, the daily highest T4 ($T4_{max}$) and T5 ($T5_{max}$) value in each 3×3 array is obtained for 13 time periods from that day. Then, if the daily temperature contrast of a 3×3 array, $T4_{max} - T4$ or $T5_{max} - T5$, is larger than 6K, the array is assumed to be cloudy.

[24] In the second step, we first calculated the standard deviation of the ch1 reflectance for the 3×3 1-km pixels array (σ_{R1}) inside each corresponding IR box. If σ_{R1} of a pixel is larger than 0.8%, the pixel is assumed to be cloud contaminated. If the cloud fraction is larger than 55% (i.e., 65 out of 144 pixels), the box is rejected. The reliability of the dust detection algorithm is checked by visually comparing selected visible images to the cloud-cleared images. Although cloud edges and optically thin clouds do pose problems, the detection algorithm captures the dust events well.

5. Results

[25] Before we compare the GOES 8 AOT retrievals with the AERONET Sunphotometer (SP) derived AOT values, it is important to examine the differences between these two retrievals. The GOES 8 has a wide field of view (roughly 1.0×1.0 km at nadir) and a broad spectral band (0.52 μm $\sim$ 0.72 μm). The SP observes on a scale of several meters with approximately 0.8° full angle field for the measurements of direct Sun and has a narrow wavelength interval on the order of 0.01μm [*Holben et al.*, 1998].

[26] In this study, because of the high temporal resolution of GOES 8 data, the time match between AERONET and GOES 8 is within 15 min. Since both SP sites in this study are close to the coast; the GOES 8 pixels that are about 8 km from the SP sites [*Moulin et al.*, 1997; *Tanré et al.*, 1997] are used in this inter-comparison to avoid contamination from the land surface, high content chlorophyll, or turbid waters [*Spinrad et al.*, 1994]. Specifically, 144 visible pixels within a 3×3 IR box centered at 17.76°N, 66.75°W and 18.28°N, 65.47°W were chosen for the LP and RR sites respectively. First the mean and standard deviation of the SP AOT in each corresponding GOES 8 observation period (±15 min) was obtained. Then we collocated these points with the GOES 8 pixels that were already cloud-cleared by using the cloud screening method described in section 4. Table 1 lists the number of points used in the cloud-clearing process. A total of 866 GOES 8 data points were obtained over the RR and LP AERONET sites, out of which 73.8% were rejected; either because the GOES 8 and SP data do not match each other within ±15 min, or because GOES 8 points have Sun glint contamination (test 1). There are also some cases where the GOES 8 has an AOT value but AERONET does not, because their cloud clearing methods

Table 1. Number of Data Points Used as a Function of the Cloud-Clearing Algorithm[a]

Site	Latitude	Longitude	Total Points	Test1	Test2	Test3	Points
Roosevelt Road	18.20°N	65.60°W	433	323	45	15	50
La Paguera	17.97°N	67.05°W	433	316	42	12	63

[a]Test1, number of points rejected due to lack of temporal collocation within ±15 min of Sunphotometer data and the Sun glint contamination; Test2, number of points rejected due to possible cloud contamination by use of IR check; Test3, number of points rejected due to the high cloud fraction determined by the ch1 3×3 standard deviation.

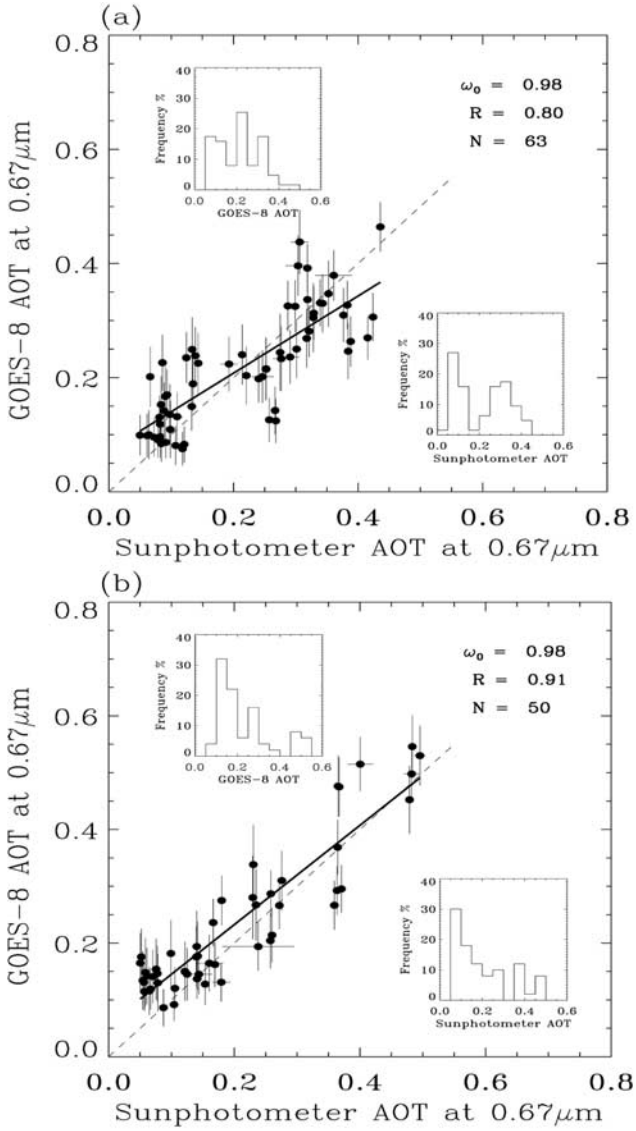

Figure 6. Comparison of dust AOT derived from GOES 8 with ground SP measurements over (a) La Paguera and (b) Roosevelt Road in Puerto Rico. The long dashed line denotes the one-to-one correspondence. The solid line is the least squares fit.

are different. Nearly 10% of the GOES 8 pixels were rejected due to the possible cloud contamination from the IR check (test 2), and 3% of the pixels were rejected due to the high cloud fraction determined from the σ_{R1} (test 3). A total of 113 points remained for the final comparisons.

[27] Figure 6 shows the scatterplot of the GOES 8 calculated AOT versus the ground-based SP AOT values for LP (Figure 6a) and RR (Figure 6b) for an effective ω_0 (at 0.67 μm) value of 0.98. The vertical and horizontal error bars denote the standard deviation in space (GOES 8, 3 × 3 IR box) and time (SP, within ±15 min). The lack of a horizontal bar indicates that the standard deviation is small. Also shown in the inset of Figures 6a and 6b are the frequency distributions of the SP and GOES 8 retrieved AOT for each site. For LP the mean and standard deviation of GOES 8 and SP AOT in Figure 6a are 0.22 ± 0.12 and 0.22 ± 0.10, respectively, with a linear correlation coefficient of 0.80. The mean and standard deviation of the GOES 8 and SP AOT values for RR site in Figure 6b are 0.19 ± 0.13 and 0.23 ± 0.13, respectively, with a linear correlation coefficient of 0.91. Considering the GOES 8 detection limit (0.04), the GOES 8 retrievals are in good agreement with SP derived values. The AOT spatial variations from GOES 8 retrievals are larger than the temporal variations of SP AOTs and the regression lines show that the GOES 8 AOTs over estimate the SP AOTs on the order of 0.06 ∼ 0.08 in low AOT conditions. One possible explanation for this is that there is still residual coastal effect which result in relative large variation of surface, and this residual effect could be dominant uncertainties in the low AOT conditions.

[28] To further validate the GOES 8 retrievals, we compare the AATS-6 aircraft-derived AOT [*Livingston et al.*, 2003] with the GOES 8 AOT values. Thirteen AATS-6 points were obtained from 21 flights when the Navajo flew within 100 m of the ocean surface and the flight time is centered on GOES 8 half-hourly observation times within 2 min. However, by restricting the analysis to cases where GOES 8 pixels are within the area of AATS-6 measurements, three points were rejected. One is due to the lack of corresponding GOES 8 data and the other two are labeled as cloudy pixels by our algorithms. The remaining 10 points are then compared with the mean GOES 8 AOT values in the Navajo 2-min flight regions. Figure 7 shows that the GOES 8 AOT has a good linear relationship with AATS-6 measurement (R = 83%). However the GOES 8 AOT values systemically overestimated the AATS-6 AOT by about 0.09. Such overestimation could originate from the subpixel cloud effect and the uncertainties of the aerosol model used in the retrievals (see section 6). On the other hand, the AATS-6 measured AOT is the mean AOT over the aircraft flight line, while the GOES 8 measured is the AOT values

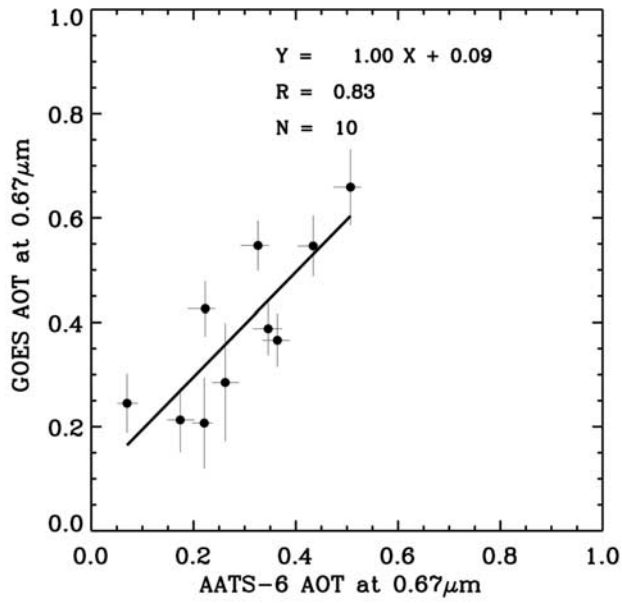

Figure 7. Comparison of dust AOT derived from GOES 8 with the aircraft AATS-6 measurements. The solid line is the least squares fit. The AATS-6 AOT at 0.67 μm is calculated using a cubic spline fit.

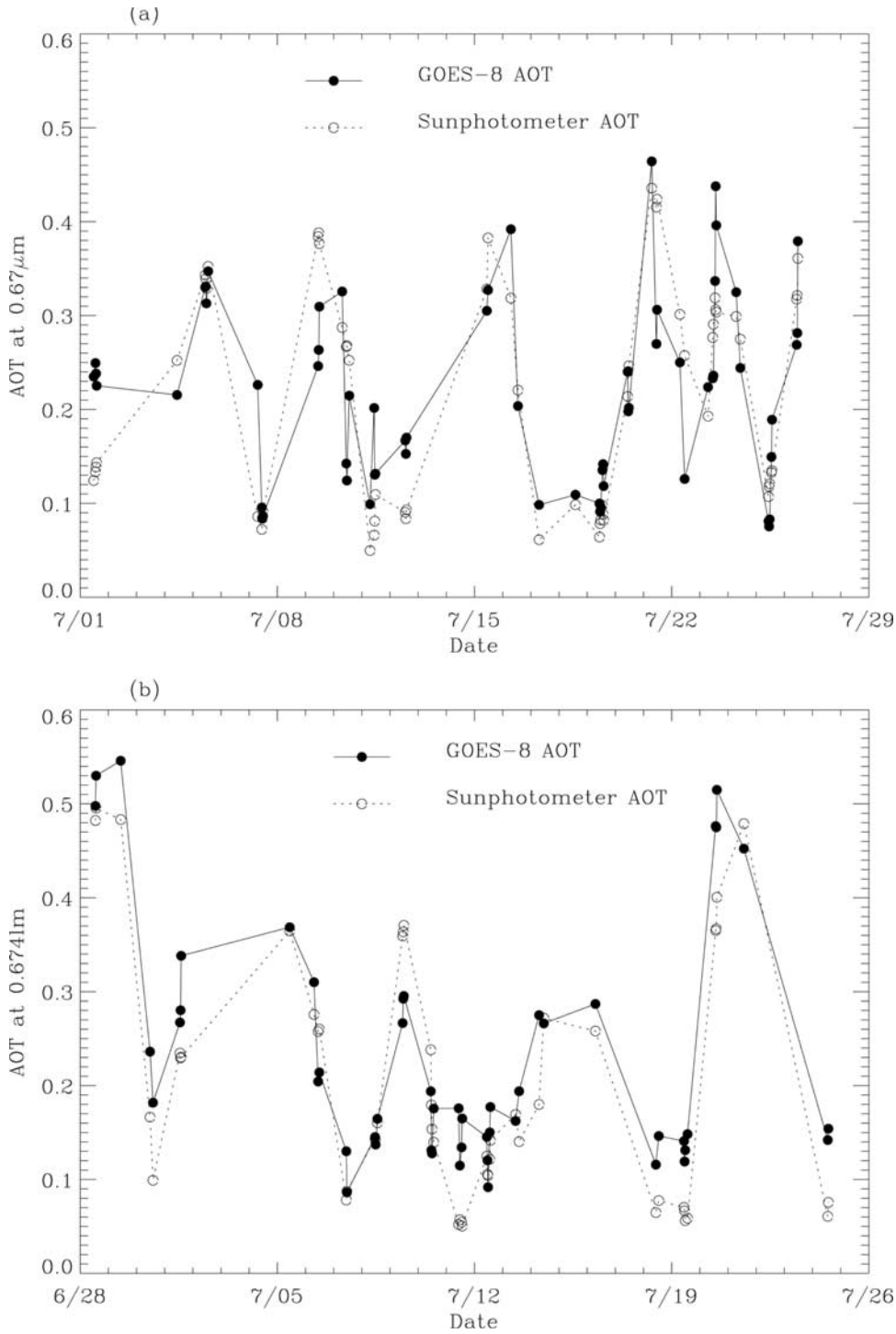

Figure 8. Scatterplot of dust optical thickness from GOES 8 retrieval and the AERONET measurements versus time over (a) La Paguera and (b) Roosevelt Road in Puerto Rico.

in the area of at least one GOES 8 pixel (about 1 km^2). Therefore GOES 8 AOT has a larger standard deviation of about 0.05 in Figure 7.

[29] Since a polar orbiting satellite, such as the AVHRR, passes through a specific area once during the day in the tropical regions, it can capture only one phase of any AOT diurnal cycle. If the area is covered by Sun glint or clouds, the possibility of daily observation will be decreased. For example, the daily mean AOT at Roosevelt Road is 0.35 with daily variations of 0.21 (from 0.24 to 0.45) on 20 July 2000. Because of the high temporal resolution of the GOES 8 imager, more opportunities are available for observing aerosols and retrieving AOT. Figures 8a and 8b show the AOT retrievals from GOES 8 retrieval and the AERONET measurements versus time over LP and RR in Puerto Rico, respectively. These results show that the GOES 8 imager has the ability to capture the diurnal AOT variations. For instance, the SP on LP site reported changes in AOT on

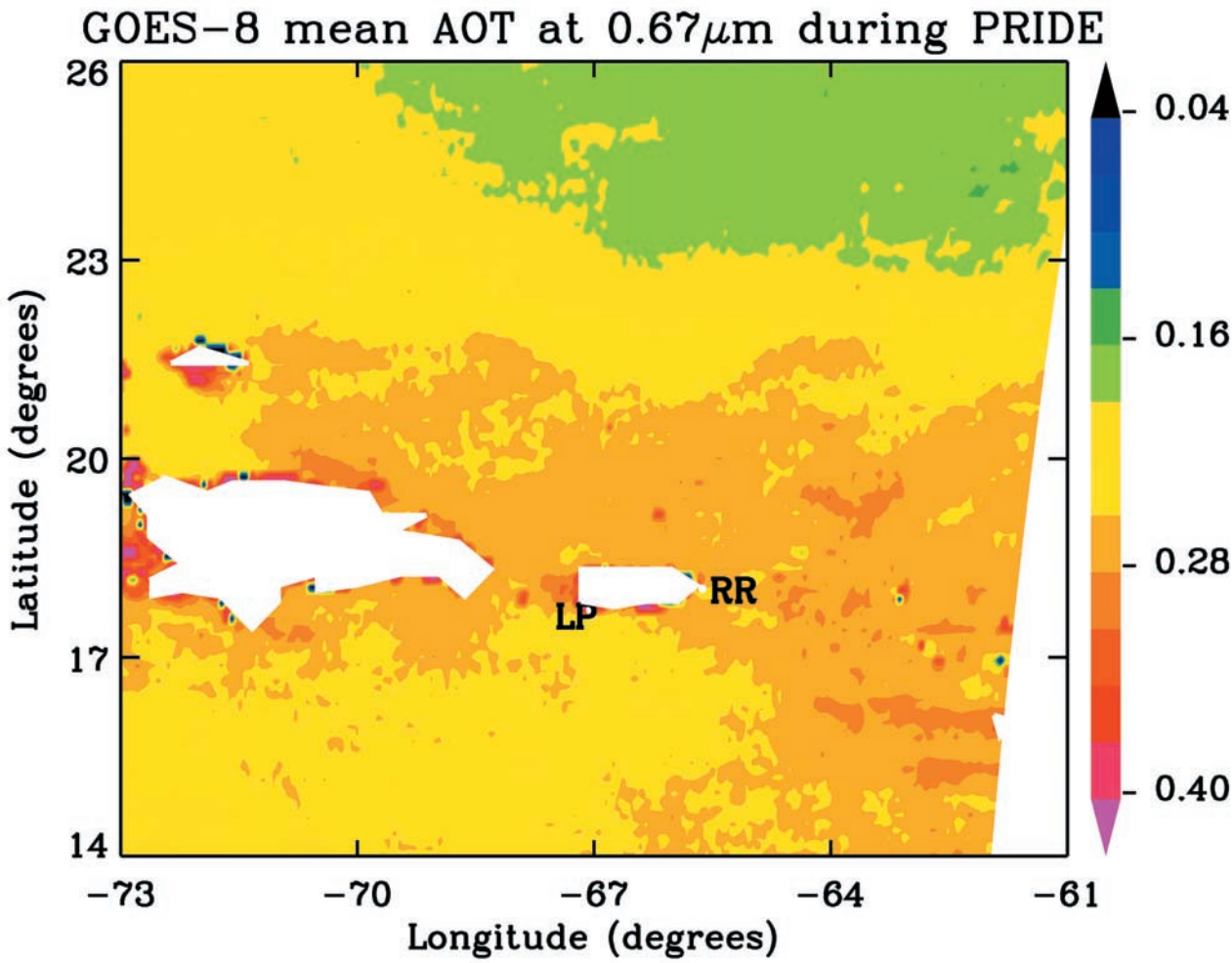

Figure 9. Monthly mean AOT at 0.67 μm derived from GOES 8 near Puerto Rico regions during PRIDE period.

23 July 2000 from 0.19 at 1301 UTC to 0.31 at 1901 UTC. The GOES 8 retrieved AOT values varied from 0.22 to 0.33 during this time. However, there are several GOES 8 AOT values that overestimate the SP derived AOT. This could be due to cloud contamination or other uncertainties (see section 6).

[30] The monthly mean AOT derived from the GOES 8 imager over the study region during PRIDE is shown in Figure 9. The spatial distribution of AOT shows high values of AOT in the southeast corner and low AOT in the northwest corner. This spatial distribution shows the effect of northeast trade wind on the dust transport [*Westphal et al.*, 1987; *Prospero*, 1999]. The dust circulates clockwise around the semipermanent "Bermuda" high-pressure center (22°N, 62°W) during each summer (see Figure 1) [*Perry et al.*, 1997; *Rapp*, 1976]. The spatial distribution in Figure 9 is consistent with results from the AVHRR optical thickness product [*Stowe et al.*, 1997] shown by *Reid et al.* [2003a]. The monthly mean GOES AOT value in the study area is 0.26 which is also consistent with AVHRR monthly mean AOT of 0.25 at the Puerto Rico region in July 2000 [*Reid et al.*, 2003a]. The averaged AOT in the study area shows a diurnal cycle with minimum at local noon and maximum in the early morning and later afternoon [*Christopher et al.*, 2003].

6. Sensitivity Analysis

[31] In this section we discuss the sensitivity of the AOT retrievals due to assumptions made in the aerosol model and surface conditions. Although sea surface is dark in the visible and is assumed to be a Lambertian reflector in the area outside of Sun glint, several factors could change the sea surface reflectance. These factors include the wind speed and its consequent white caps effect; the residual Sun glint contamination effect; the change of the light leaving the water coming from beneath the sea surface due to chlorophyll content or high turbidity coastal waters. The reflectance uncertainty from underlight is about 0.14 ± 0.06% for most open oceans with pigment concentration less than 0.25 mg m^{-3} [*Gordon and Morel*, 1983], and can be as high as 0.55 ± 0.5% [*Ignatov et al.*, 1995] or 1% [*Wagener et al.*, 1997] in coastal ocean with high pigment content. The reflectance from foam under normal sea wind conditions ranges from 0.03 ± 0.05% [*Ignatov et al.*, 1995] or 0.06 ± 0.04% [*Wagener et al.*, 1997]. It could be as

high as 1% when sea surface wind speed exceeds 15 m s^{-1} [*Gregg and Carder*, 1990]. On the basis of these studies, the variation of the sea surface reflectance is 0.2% $\sim$ 0.4% in normal conditions, and can reach 1% in some extreme conditions (e.g., high sea surface wind larger than 15 m s^{-1} or very high pigment content much larger than 0.25 mg m^{-3}).

[32] To examine the change in GOES 8 retrieved AOT due to ρ_s, we change ρ_s by ±1%. When AOT is small (<0.2), the single scattering processes will dominate, which implies a linear relationship between ρ_s and TOA reflectance. A 1% change in ρ_s appeared to cause the retrieved AOT to change by 0.1 and is similar to the result obtained by *Wagener et al.* [1997]. The maximum absolute retrieval error in this study due to the uncertainty of the sea surface is 0.1, with an average error of 0.02 $\sim$ 0.04 when a normal variation of 0.2–0.4% in ρ_s is considered.

[33] The real component (N_r) of the dust refractive index ranges from 1.50 to 1.56 in the visible spectrum [*Patterson et al.*, 1977]. The typical value of N_r for the aerosol retrieval over ocean is 1.50 [*Ignatov et al.*, 1995; *Wagener et al.*, 1997; *Mishchenko et al.*, 1999; *Higurashi and Nakajima*, 1999]. Previous studies have used N_r values of 1.53 [*Kaufman et al.*, 2000] and 1.54 [*Sokolik et al.*, 2001] for Saharan dust. Thereby the relative uncertainty of N_r is small ($dN_r/N_r <$ 0.01) compared to variations of N_i, As discussed in section 3, there is a large range of values reported in the literature for the imaginary component (N_i) of the dust aerosol refractive index. In previous satellite retrieval algorithms, the aerosols over ocean were assumed to be nonabsorbing [*Rao et al.*, 1989]. However, a survey of N_i values from early light-attenuation measurements shows that N_i may have a large range from 0.009 to 0.003 or less depending on different chemical compositions and geographic locations [*Sokolik et al.*, 1993]. Recently, the retrieval of N_i from remote sensing measurements showed that the dust aerosols have reduced absorption in the blue spectrum [*Kaufman et al.*, 2001; *Moulin et al.*, 2001]. However, this discrepancy may be due to the measurements and the mixing of the nonabsorbing aerosols [*Sokolik et al.*, 1993; *Mishchenko et al.*, 1999]. In this study, a N_i value of 0.0015 was used. This value was derived from the light-scattering and light-attenuation measurements, which is the effective imaginary component of the refractive index in the sample volume.

[34] To evaluate the effect of N_i on our retrievals, we change the original N_i (*0.0015*) from 0.003 to zero, while keeping the size distribution the same. Our calculations show that AOT could increase by 0.05 as N_i decreases by 0.0015, and vice versa**.** A change in N_i from 0.003 to zero leads to a change in the effective ω_0 value from 0.96 to 1.00. This will yield a mean AOT in Figure 6b ranging from 0.28 to 0.18. The sensitivity of the retrieved optical thickness to N_i can be defined as $(\Delta\tau/\tau)/(\Delta Ni/Ni)$. If N_i is fixed at 0.015, our results show that the sensitivity could be 100% for τ less than 0.1 and 20% for τ around 0.5. Since AOT was less than 0.5 and the averaged value is around 0.25 during PRIDE, we conclude that our absolute error ($\Delta\tau$) due to uncertainties in N_i is less 0.1 and mean error is about 0.05. However the relative error ($\Delta\tau/\tau$) is very sensitive for small AOT retrievals and using a fixed, globally uniform value of refractive index may result in significant retrieval errors, especially for low aerosol loading [*Mishchenko et al.*, 1999].

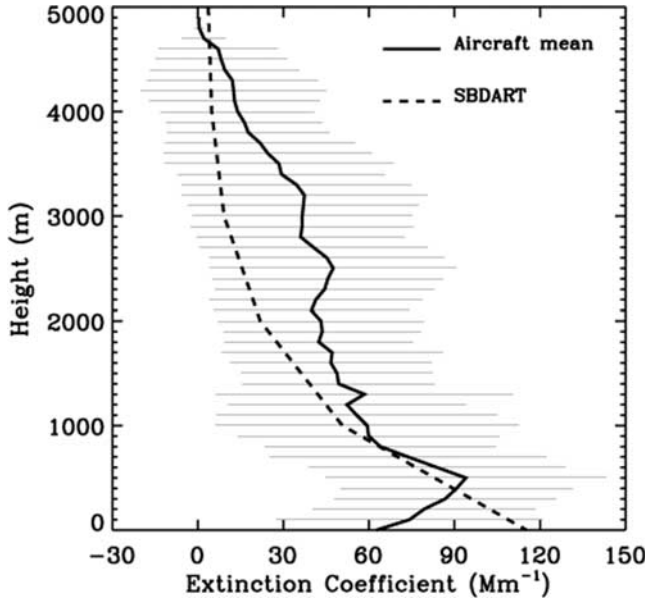

Figure 10. Averaged aerosol extinction coefficient vertical profile during PRIDE and the default profile used in DISORT. The horizontal lines are standard deviation for each layer.

[35] The radiative transfer model used in this study considers the multiple scattering of the aerosols, gas absorption, and molecular scattering and has been well validated [*Ricchiazzi et al.*, 1998]. Our radiative transfer calculations do not consider the effect of polarization. *Wagener et al* [1997] found that by neglecting the multiple scattering and polarization effects in radiative transfer calculations could result in overestimation of AVHRR AOT retrievals by about 0.015 for AOT less 1. In our retrievals, we have included multiple scattering, and we expect the uncertainties due to polarization to be less than 0.003 for AOT values less than 0.5**.** The atmospheric temperature and water vapor profile in our model is the standard tropical summer profile [*McClatchey et al*., 1972]. The difference in temperature and water vapor values at each layer between the tropical summer profile and the aircraft measured profiles [*Reid et al.*, 2003a] are less than 2%. Therefore the retrieval uncertainties in AOT due to the assumed tropical water vapor loading are small. A typical value of stratosphere AOT has also been considered directly in the radiative transfer model [*Ricchiazzi et al.*, 1998]. Since the important gas absorption in GOES 8 ch1 are H_2O and O_3, the other uncertainties in the radiative transfer model are due to the variations in ozone and the aerosol vertical profile. As *Wagener et al.* [1997] noted, the standard deviation of the ozone optical depth over the North Atlantic oceans is around 0.002 and this effect on AOT retrieval is negligible. We therefore address the uncertainties in GOES 8 retrieved AOT due to the assumed aerosol vertical profile.

[36] The aerosol extinction coefficient vertical profile in our radiative transfer model varies exponentially with height [*Ricchiazzi et al.*, 1998]. However, it has been observed by

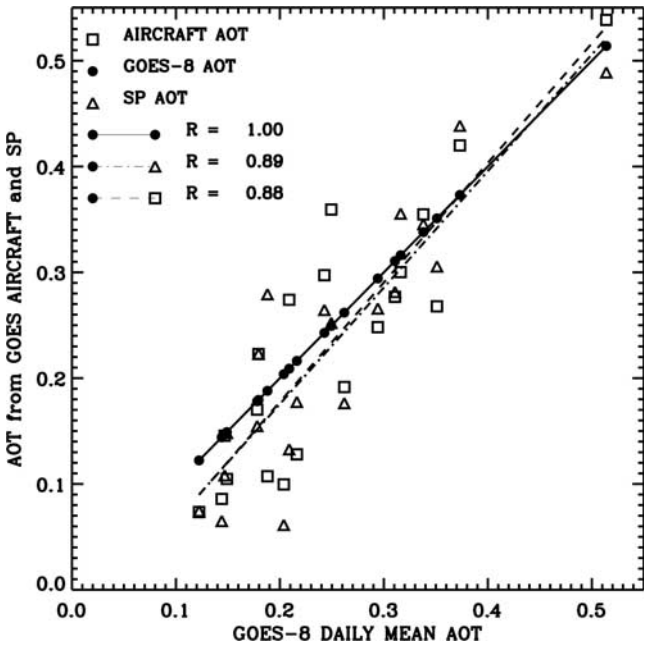

Figure 11. Comparison of daily mean dust AOT from GOES 8 with ground SP measurements and aircraft measurements. The solid line denotes the one-to-one correspondence. The dashed line is the least squares fit between aircraft AOT and GOES 8 AOT. The dot-dashed line represents the least squares fit between SP AOT with the GOES 8 AOT.

lidar measurements [*Chazette et al.*, 1998; *Hamomou and Chazette*, 1998] and balloon-borne scattering measurements [*Dulac and Chazette*, 1998] that aerosols are often observed in complex multilayer structures. The Lidar In-Space Technology Experiment also has shown that the Saharan dust layer is inhomogeneous and often characterized by several dust and cloud layers [*Winker et al.*, 1996]. Figure 10 shows the aircraft-derived vertical profile of aerosol extinction coefficient and the default extinction coefficient profile used in the DISORT model. The PRIDE observations show that the maximum value of the projected-average extinction coefficient profile is not at the surface, but 500 m above the surface and higher when an elevated dust layer is present [*Reid et al.*, 2003a]. Our calculation shows that the differences in GOES 8 retrieved AOT when using the default vertical extinction profile and the aircraft-inferred profile are on the order of 0.005 because the effective ω_0 values used for each layer are the same. To model the radiative properties of mixed-aerosols, the size distribution, vertical distribution, and the refractive index of different aerosol species are needed [*Quijano et al.*, 2000]. Currently, this type of data is not available, and therefore the effect of inhomogeneity cannot be estimated. Another way to check the reliability of the vertical homogeneity assumption in our retrievals is to compare the GOES 8 AOT with the AERONET SP AOT and the AOT calculated from aircraft-derived extinction profile. Figure 11 shows that the comparisons between different independent measurements are in good agreement. For example, using daily averages over the RR and LP sites, the linear correlation coefficient (R) between GOES 8 and AOT calculated from extinction profile is 0.88 while R is 0.89 between the GOES 8 and AERONET derived values.

[37] Dust aerosols are made of several minerals and have irregular shapes [*Kalashnikova and Sokolik*, 2002; *Mishchenko et al.*, 1995]. Although new methods have been proposed to calculate the optical properties of nonspherical particles [*Wiscombe and Mugnai*, 1988; *Mishchenko et al.*, 1995] these calculations are seldom used in satellite retriev-

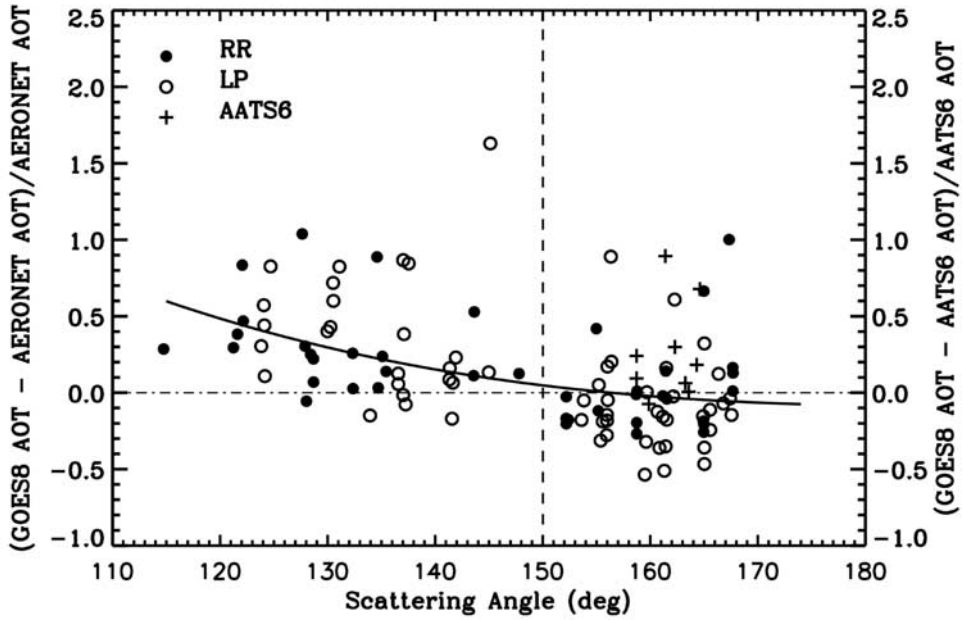

Figure 12. Relative errors as a function of scattering angles between (a) GOES 8 and SP AOT at two AERONET sites (RR and LP) and (b) GOES 8 and AATS6 AOT. A third-order polynomial fit is also shown. The dot-dashed line is the zero bias line.

als due to the difficulties in accurately describing particle shape parameters. Most satellite retrieval algorithms use Mie calculations [e.g., *Tanré et al.*, 1997; *Kaufman et al.*, 1997, 2000, 2001]. There are small differences for optical cross sections and single scattering albedos between spherical and nonspherical particles when r_{eff} and the refractive index are the same [*Mishchenko et al.*, 1997]. Compared to the phase function of spherical particles, the phase function of nonspherical particles is much larger at the scattering angle from $90° \sim 150°$ and much smaller at scattering angle from 150° to 180° [*Mishchenko et al.*, 1997]. The difference in phase function between spherical and nonspherical particles become larger for larger r_{eff}, and will result in errors in the AOT retrievals of nonspherical aerosols from radiance measurements. [*Mishchenko et al.*, 1997]. *Levy et al.* [2003] note that the overestimation of the MODIS retrievals when compared to the AATS-6 AOT values are largely due to the nonspherical effect of dust aerosols. To examine the nonspherical effect of dust aerosols, we analyze the scattering angle versus relative error (Figure 12) for the two AERONET sites and the AATS AOT values for cases where SP and AATS6 AOTs are larger than background values of 0.07 [*Reid et al.*, 2003a]. Figure 12 shows that for scattering angles less than 150°, GOES 8 AOT systematically overestimate SP AOT and for scattering angle larger than 150°, the GOES 8 AOT slightly underestimate SP AOT. These results generally agree with previous theoretical studies [*Mishchenko et al.*, 1997] where the spherical-nonspherical differences in phase functions changes sign around scattering angle values of 150° and such difference would result in uncertainties in AOT retrievals from radiance measurements. The relative error between GOES 8 and AATS6 AOT are smaller when compared with the GOES 8 vs. AERONET values although the range of scattering angles are small in this comparison. These relative errors are due to a combination of assumptions from sphericity, surface and aerosol model effects and further research is needed to quantify the effect of non sphericity on GOES 8 retrievals.

7. Summary and Conclusions

[38] Using measured aerosol size distributions in Mie calculations, a refractive index value of 1.53–0.0015i provides the best fit with light scattering and absorption measurements during PRIDE. A qualognormal size distribution with an r_{eff} value of 0.72μm provided an effective single scattering albedo value of 0.98 at 0.67 μm that is consistent with recent studies [*Kaufman et al.*, 2001; *Moulin et al.*, 2001]. The look-up table is then constructed by using the results of the Mie calculation in the DISORT model. A stringent cloud mask and dust detection algorithm is developed by use of multiple channels, spatial and temporal tests from the GOES 8 imager. Although GOES 8 visible channel has undergone significant degradation since launch, our retrieved AOT from the recalibrated GOES 8 ch1 reflectance are in good agreement with AERONET values. The GOES 8 monthly mean retrieved AOT (0.19 ± 0.13 and 0.22 ± 0.12) matches the monthly mean AOT from the ground-based SP observations (0.23 ± 0.13 and 0.22 ± 0.10).

[39] Since GOES 8 only has one visible channel, it is necessary to make assumptions or use measurements to describe other parameters including size distribution, refractive index, and surface reflectance. The main uncertainties in the GOES 8 retrieved AOT are due to assumptions in N_i ($\Delta\tau = \pm 0.05$) and ρ_s [$\Delta\tau = \pm(0.02 \sim 0.04)$]. The total uncertainties are $\pm(0.03 \sim 0.09)$ with average value of ±0.06. In another paper, the GOES 8 derived values of AOT are used to calculate the radiative forcing of dust aerosols both at the top of atmosphere and at the surface [*Christopher et al.*, 2003]. Furthermore, the geostationary imagers provide valuable information in providing the diurnal variability of dust aerosols.

[40] **Acknowledgments.** This research was partially supported by NASA grant NCC 8141 (Global Aerosol Climatology Project), NASA's IDS program (FLAMBE) and was part of Jun Wang's master's thesis. The AATS-6 measurements and analyses were supported by the Global Aerosol Climatology Project and NASA's Earth Observing System Inter-Disciplinary Science (EOS-IDS) Program. The GOES data were obtained through the Global Hydrology and Climate Center. We thank U. S. Nair for providing the GOES calibration code. We also thank Kevin Laws for his help with Figure 1.

References

Anderson, T. L., and J. A. Ogren, Determining aerosol radiative properties using the TSI 3563 integrating nephelometer, *Aerosol Sci. Technol.*, *29*, 57–69, 1998.

Anderson, T. L., et al., Performance characteristics of a high sensitivity, three-wave length total scatter/backscatter nephelometer, *J. Atmos. Oceanic. Technol.*, *13*, 967–986, 1996.

Carlson, T. N., and S. G. Benjamin, Radiative heating rates for Saharan dust, *J. Atmos. Sci.*, *37*, 193–213, 1980.

Claquin, T., M. Schulz, Y. J. Balkanski, and O. Boucher, Uncertainties in assessing radiative forcing by mineral dust, *Tellus, Ser. B*, *50*, 491–505, 1998.

Chazette, P., et al., Infrared radiative forcing of a Sahara dust plume in the North Atlantic, *J. Aerosol Sci.*, *29*, S130–S132, 1998.

Christopher, S. A., and J. Zhang, Daytime variation of shortwave direct radiative forcing of biomass burning aerosols from GOES 8 imager, *J. Atmos. Sci.*, *59*, 681–691, 2002.

Christopher, S. A., J. Chou, J. Zhang, X. Li, and R. M. Welch, Shortwave direct radiative forcing of biomass burning aerosols estimated from VIRS and CERES data, *Geophys. Res. Lett.*, *27*, 2197–2200, 2000.

Christopher, S. A., J. Zhang, B. N. Holben, and S.-K. Yang, GOES-8 and NOAA-14 AVHRR retrieval of smoke aerosol optical thickness during SCAR-B, *Int. J. Remote Sens.*, in press, 2002.

Christopher, S. A., J. Wang, Q. Ji, and S.-C. Tsay, Estimation of diurnal shortwave dust aerosol radiative forcing during PRIDE, *J. Geophys. Res.*, *108*, doi:10.1029/2002JD002787, in press, 2003.

Chu, D. A., Y. J. Kaufman, C. Ichoku, L. A. Remer, D. Tanré, and B. N. Holben, Validation of MODIS aerosol optical depth retrieval over land, *Geophys. Res. Lett.*, *29*(12), 8007, doi:10.1029/2001GL013205, 2002.

Cox, C., and W. Munk, Measurements of the roughness of sea surface from the Sun's glitter, *J. Opt. Soc. Am.*, *44*, 838–850, 1954.

D'Almeida, G. A., On the variability of desert aerosol radiative characteristics, *J. Geophys. Res.*, *92*, 3017–3026, 1987.

Davies, C. N., Size distribution of atmospheric particles, *J. Aerosol. Sci.*, *5*, 293–300, 1974.

Diner, D. J., et al., MISR aerosol optical thickness depth retrievals over southern Africa during the SAFARI-2000 dry season campaign, *Geophys. Res. Lett.*, *28*, 3127–3130, 2001.

Duce, R., Distributions and fluxes of mineral aerosol, in *Aerosol Forcing of Climate*, edited by R. J. Charlson and J. Heintzenberg, pp. 43–72, John Wiley, New York, 1995.

Dulac, F., and P. Chazette, Balloonborne profiling of African dust over the tropical Atlantic, *J. Aerosol Sci.*, *29*, S1265–S1266, 1988.

Ellrod, G. P., R. V. Achutunl, J. M. Daniels, E. M. Prints, and J. P. Nelson III, An assessment of GOES-8 imager data quality, *Bull. Am. Meteorol. Soc.*, *79*, 2509–2526, 1998.

Fouquart, Y., B. Bonnel, G. Bogniez, J. C. Buriez, L. Smith, J. J. Morcrette, and A. Cerf, Observations of Sahara aerosols, results of ECLATS field experiment, part II: Broadband radiative characteristics of the aerosols and vertical radiative flux divergence, *J. Clim. Appl. Meteorol.*, *26*, 38–52, 1987.

Geogdzhayev, I. V., M. I. Mishchenko, W. B. Rossow, B. Cairns, and A. A. Lacis, Global two-channel AVHRR retrievals of aerosol properties over the ocean for the period of NOAA-9 observations and preliminary retriev-

als using NOAA-7 and NOAA-11 data, *J. Atmos. Sci.*, *59*, 262–278, 2002.

Gordon, H. R., and A. Y. Morel, *Remote Assessment of Ocean Color for Interpretation of Satellite Visible Imagery: A Review*, 114 pp., Springer-Verlag, New York, 1983.

Greenwald, T. J., and S. A. Christopher, The GOES-IM imager: New tools for studying the microphysical properties of boundary layers clouds, *Bull. Am. Meteorol. Soc.*, *81*, 2607–2619, 2000.

Gregg, W. W., and K. L. Carder, A simple spectral solar irradiance model for cloudless maritime atmosphere, *Limnol. Oceanogr.*, *35*, 1657–1675, 1990.

Hamomou, E., and P. Chazette, Evidence of Sahara mineral aerosol transport to the Mediterranean inside well-defined layers, *J. Aerosol Sci.*, *29*, S1263–S1264, 1998.

Hasen, J. E., and A. A. Lacis, Sun and dust versus greenhouse gases: An assessment of their relative roles in global climate change, *Nature*, *346*, 713–719, 1990.

Higurashi, A., and T. Nakajima, Development of a two-channel aerosol retrieval algorithm on a global scale using NOAA AVHRR, *J. Atmos. Sci.*, *56*, 924–941, 1999.

Holben, B. N., et al., AERONET—A federal instrument network and data archive for aerosol characterization, *Remote Sens. Environ.*, *66*, 1–16, 1998.

Ignatov, A. M., L. L. Stowe, S. M. Sakerin, and G. K. Korotaev, Validation of the NOAA/NESDIS satellite aerosol product over the North Atlantic in 1989, *J. Geophys. Res.*, *100*, 5123–5132, 1995.

Ignatov, A. M., and L. L. Stowe, Physical basis, premise, and self-consistency of aerosol retrievals from TRMM VIRS, *J. Appl. Meteorol.*, *39*, 2257–2277, 2000.

Intergovernmental Panel on Climate Change (IPCC), *Climate Change 2001: The Scientific Basis, Contribution of Working Group I to the Third Assessment Report of the Intergovernmental Panel on Climate Change*, edited by J. T. Houghton et al., Cambridge Univ. Press, New York, 2001.

Jankowiak, I., and D. Tanré, Satellite climatology of Saharan dust outbreaks: Method and preliminary results, *J. Clim.*, *5*, 646–656, 1992.

Kalashnikova, O. V., and I. N. Sokolik, Importance of shapes and compositions of wind-blown dust particles for remote sensing at solar wavelengths, *Geophys. Res. Lett.*, *29*(10), 1398, doi:10.1029/2002GL014947, 2002.

Kaufman, Y. J., and T. Nakajima, Effect of Amazon smoke on cloud microphysics and albedo-analysis from satellite imagery, *J. Appl. Meteorol.*, *32*, 729–744, 1993.

Kaufman, Y. J., D. Tanré, L. A. Remer, E. F. Vermote, A. Chu, and B. N. Holben, Operational remote sensing of tropospheric aerosol over land from EOS moderate resolution imaging spectroradiometer, *J. Geophys. Res.*, *102*, 17,051–17,067, 1997.

Kaufman, Y. J., A. Karnieli, and D. Tanré, Detection of dust over deserts using satellite data in the solar wavelengths, *IEEE Trans. Geosci. Remote Sens.*, *38*, 525–531, 2000.

Kaufman, Y. J., D. Tanre, O. Dubovik, A. Karnieli, and L. A. Remer, Absorption of sunlight by dust as inferred from satellite and ground-based remote sensing, *J. Geophys. Lett.*, *28*, 1479–1482, 2001.

Karyampudi, V. M., et al., Validation of the Saharan dust plume conceptual model using Lidar, Meteosat, and ECMWF data, *Bull. Am. Meteorol. Soc.*, *80*, 1045–1075, 1999.

King, M. D., Y. J. Kaufman, D. Tanre, and T. Nakajima, Remote sensing of tropospheric aerosols from space: Past, present, and future, *Bull. Am. Meteorol. Soc.*, *80*, 2229–2259, 1999.

Knapp, K. R., T. H. Vonder Haar, and Y. J. Kaufman, Aerosol optical depth retrieval from GOES-8: Uncertainty study and retrieval validation over South America, *J. Geophys. Res.*, *107*(D7), 4055, doi:10.1029/2001JD000505, 2002.

Levin, Z., J. H. Joseph, and Y. Mekler, Properties of Sharav (Khamsin) dust—Comparison of optical and direct sampling data, *J. Atmos. Sci.*, *27*, 882–891, 1980.

Levy, R., L. A. Remer, D. Tanre, Y. J. Kaufman, C. Ichoku, B. Holben, J. Livingston, P. B. Russell, and H. Maring, Evaluation of the MODIS retrievals of dust aerosol over the ocean during PRIDE, *J. Geophys. Res.*, *108*(D19), 8594, doi:10.1029/2002JD002460, in press, 2003.

Liao, H., and J. H. Seinfeld, Radiative forcing by mineral dust aerosols: Sensitivity to key variables, *J. Geophys. Res.*, *103*, 31,637–31,645, 1998.

Liu, X., J. Wang, and S. A. Christopher, Shortwave direct radiative forcing of Saharan dust aerosols over the Atlantic Ocean, *Int. J. Remote Sens.*, in press, 2003.

Livingston, J. M., et al., Airborne Sun photometer measurements of aerosol optical depth and columnar water vapor during the Puerto Rico Dust Experiment and comparison with land, aircraft, and satellite measurements, *J. Geophys. Res.*, *108*(D19), 8588, doi:10.1029/2002JD02520, 2003.

Maring, H., D. L. Savoie, M. A. Izaguirre, C. McCormick, R. Arimoto, J. M. Prospero, and C. Pilinis, Aerosol physical and optical properties and their relationship to aerosol composition in the free troposhpere at Izana, Tenerife, Canary Islands, during July 1995, *J. Geophys. Res.*, *105*, 14,677–14,700, 2000.

Matsumoto, T., P. B. Russell, C. Mina, W. Van Ark, and V. Banta, Airborne tracking Sunphotometer, *J. Atmos. Oceanic Technol.*, *4*, 336–339, 1987.

McClatchey, R. A., R. W. Fenn, J. E. A. Selby, F. E. Volz, and J. S. Garing, Optical properties of the atmosphere, *Rep. AFCRL-TR-71-0279, Environ. Res. Pap. 354*, Air Force Cambridge Res. Lab., Bedford, Mass., 1971.

Menzel, W. P., and J. F. Purdom, Introducing GOES-I: The first of a new generation of geostationary operational environmental satellite, *Bull. Am. Meteorol. Soc.*, *75*, 757–781, 1994.

Mishchenko, M. I., A. A. Lacis, B. E. Carlson, and L. D. Travis, Nonsphericity of dust-like tropospheric aerosols: Implications for aerosol remote sensing and climate modeling, *Geophys. Res. Lett.*, *22*, 1077–1080, 1995.

Mishchenko, M. I., L. D. Travis, R. A. Kahn, and R. A. West, Modeling phase functions for dust-like tropospheric aerosols using a shape mixture of randomly oriented polydisperse spheroids, *J. Geophys. Res.*, *102*, 16,831–16,847, 1997.

Mishchenko, M. I., I. V. Geogdzhayev, B. Cairns, W. B. Rossow, and A. Lacis, Aerosol retrievals over ocean by use of channels 1 and 2 AVHRR data: Sensitivity analysis and preliminary results, *Appl. Opt.*, *38*, 7325–7341, 1999.

Moulin, C., F. Dulac, C. E. Lambert, P. Chazette, I. Jankowiak, B. Chatenet, and F. Lavenn, Long-term daily monitoring of Sahara dust load over ocean using Meteosat ISSCP-B2 data: 2. Accuracy of the method and validation using Sun photometer measurements, *J. Geophys. Res.*, *102*, 16,959–16,969, 1997.

Moulin, C., H. R. Gordon, V. F. Banzon, and R. H. Evans, Assessment of Sahara dust absorption in the visible from SeaWiFS imagery, *J. Geophys. Res.*, *106*, 18,239–18,250, 2001.

Patterson, E. M., Optical properties of the crustal aerosol: Relation to chemical and physical characteristics, *J. Geophys. Res.*, *86*, 3236–3246, 1981.

Patterson, E. M., D. A. Gillette, and B. H. Stockton, Complex index of refraction between 300 nm and 700 nm for Sahara aerosols, *J. Geophys. Res.*, *82*, 3153–3160, 1977.

Perry, K. D., T. A. Cahill, R. A. Eldred, and D. D. Dutcher, Long-range transport of North African dust to the eastern United States, *J. Geophys. Res.*, *102*, 11,225–11,238, 1997.

Prins, E. M., J. M. Feltz, W. P. Menzel, and D. E. Ward, An overview of GOES—Diurnal fire and smoke results for SCAR-B and the 1995 fire season in South America, *J. Geophys. Res.*, *103*, 31,821–31,836, 1998.

Prospero, J. M., Long-term measurements of the transport of African minerals dust to the southeastern United States: Implications for regional air quality, *J. Geophys. Res.*, *104*, 15,917–15,927, 1999.

Quijano, A. L., I. N. Sokolik, and O. B. Roon, Influence of the aerosol vertical distribution on the retrievals of aerosol optical thickness from satellite radiance measurements, *Geophys. Res. Lett.*, *27*, 3460–3475, 2000.

Rao, C. R. N., L. Stowe, and P. McClain, Remote sensing of aerosols over oceans using AVHRR data, theory, practice and application, *Int. J. Remote Sens.*, *10*, 743–749, 1989.

Rao, C. R. N., J. Chen, and N. Zhang, Calibration of the visible channel of the GOES imager using the advanced very high resolution radiometer, paper presented at 10th Conference on Atmosphere Radiation, Am. Meteorol. Soc., Madison, Wisc., 1999.

Rapp, A., *Can Desert Encroachment Be Stopped? A Study With Emphasis on Africa*, *Ecol. Bull.*, vol. 24, edited by A. Rapp, H. N. Le Houerou, and B. Lundholm, Swed. Nat. Sci. Res. Counc., Stockholm, 1976.

Reid, J. S., et al., Analysis of measurements of Saharan dust by airborne and ground-based remote sensing methods during the Puerto Rico Dust Experiment (PRIDE), *J. Geophys. Res.*, *108*(D19), 8586, doi:10.1029/2002JD002493, in press, 2003a.

Reid, J. S., et al., Comparison of size and morphological measurements of coarse mode dust particles from Africa, *J. Geophys. Res.*, *108*(D19), 8593, doi:10.1029/2002JD002485, in press, 2003b.

Ricchiazzi, P., S. Yang, C. Gautier, and D. Sowle, SBDART: A research and teaching software tool for plane-parallel radiative transfer in the Earth's atmosphere, *Bull. Am. Meteorol. Soc.*, *79*, 2101–2114, 1998.

Savoie, D. L., J. M. Prospero, and E. S. Saltzman, Non-sea-salt sulfate and nitrate in trade wind aerosols at Barbados: Evidence for long-range transport, *J. Geophys. Res.*, *94*, 5069–5080, 1989.

Schütz, L., and R. Jaenicke, Particle number and mass distribution above 10^{-4} cm radius in sand and aerosol of the Sahara desert, *J. Appl. Meteorol.*, *13*, 863–870, 1974.

Smirnov, A., B. N. Holben, T. F. Eck, O. Dubovik, and I. Slutsker, Cloud screening and quality control algorithms for the AERONET database, *Remote Sens. Environ.*, *73*, 337–349, 2000.

Sokolik, I. N., and O. B. Toon, Direct radiative forcing by anthropogenic mineral aerosols, *Nature*, *381*, 681–683, 1996.

Sokolik, I. N., A. Andronova, and T. C. Johnson, Complex refractive index of atmospheric dust aerosols, *Atmos. Environ.*, *27*, 2495–2502, 1993.

Sokolik, I. N., D. M. Winker, G. Bergametti, D. A. Gillette, G. Carmichael, Y. J. Kaufman, L. Gomes, L. Schütz, and J. E. Penner, Introduction to special section: Outstanding problems in quantifying the radiative impacts of mineral dust, *J. Geophys. Res.*, *106*, 18,015–18,028, 2001.

Spinrad, R. W., K. L. Carder, and M. J. Perry, *Ocean Opticals*, Oxford Univ. Press, New York, 1994.

Stowe, L. L., A. M. Ingatov, and R. R. Singh, Development, validation, and potential enhancement to the second-generation operational aerosol product at the National Environmental Satellite, Data, and Information Service of the National Oceanic and Atmospheric Administration, *J. Geophys. Res.*, *102*, 16,923–16,934, 1997.

Tanré, D., P. Y. Deschamps, C. Devaux, and M. Herman, Estimation of Sahara aerosol optical thickness from blurring effects in thematic mapper data, *J. Geophys. Res.*, *93*, 15,955–15,964, 1988.

Tanré, D., Y. J. Kaufman, M. Herman, and S. Matto, Remote sensing of aerosol properties over oceans using the MODIS/EOS spectral radiance, *J. Geophys. Res.*, *102*, 16,971–16,988, 1997.

Tegen, I., and A. A. Lacis, Modeling of particle size distribution and its influence on the radiative properties of mineral dust aerosol, *J. Geophys. Res.*, *101*, 19,237–19,244, 1996.

Torres, O., P. K. Bhartia, J. R. Herman, A. Sinyuk, P. Ginoux, and B. Holben, A long-term record of aerosol optical depth from TOMS observations and comparison to AERONET measurements, *J. Atmos. Sci.*, *59*, 398–413, 2002.

Twomey, S. A., The influence of pollution on the short wave albedo of clouds, *J. Atmos. Sci*, *34*, 1149–1152, 1977.

Volz, F. E., Spectral skylight and solar radiance measurements in the Caribbean: Maritime aerosols and Sahara dust, *J. Atmos. Sci.*, *27*, 1041–1047, 1970.

Wagener, R., S. Nemesure, and S. E. Schwartz, Aerosol optical thickness over oceans: High space- and time resolution retrieval and error-budget from satellite radiometry, *J. Appl. Meteorol.*, *14*, 577–590, 1997.

Westphal, D. L., O. B. Toon, and T. N. Carlson, A two-dimensional numerical investigation of the dynamics and microphysics of Saharan dust storms, *J. Geophys. Res.*, *92*, 3027–3049, 1987.

Winker, D. M., R. H. Couch, and M. P. McCormick, An overview of LITE: NASA's Lidar In-Space Technology Experiment, *Proc. IEEE*, *84*, 64–180, 1996.

Wiscombe, W. J., and A. Mugnai, Scattering from nonspherical Chebyshev particles, 2, Means of angular scattering patterns, *Appl. Opt.*, *27*, 2405–2421, 1988.

World Climate Program (WCP), *Aerosols and Their Climate Effects*, *Ser. Rep. 55*, edited by A. Deepak and H. E. Gerber, Int. Counc. Sci., World Meteorol. Organ., Geneva, Switzerland, 1983.

Zhang, J., S. A. Christopher, and B. Holben, Intercomparison of aerosol optical thickness derived from GOES 8 imager and ground-based Sun photometers, *J. Geophys. Res.*, *106*, 7387–7398, 2001.

S. A. Christopher and J. Wang, Department of Atmospheric Sciences, NSSTC, University of Alabama in Huntsville, 320 Sparkman Drive, Huntsville, AL 35806, USA. (sundar@nsstc.uah.edu)

J. S. Reid, Naval Research Laboratory, 7 Grace Hopper Street, Monterey, CA 93943-5502, USA.

H. B. Maring and D. L. Savoie, Rosenstiel School of Marine and Atmospheric Science, University of Miami, Miami, FL 33149, USA.

B. N. Holben, Biospheric Sciences Branch, NASA Goddard Space Flight Center, Greenbelt, MD 20771, USA.

J. M. Livingston, SRI International, 333 Ravenswood Avenue, Menlo Park, CA 94025, USA.

P. B. Russell, NASA Ames Research Center, Moffett Field, CA 94035, USA.

S.-K. Yang, Climate Prediction Center, NCEP W/NP53, World Weather Building, 5200 Auth Road, Washington, DC 20233, USA.